Draft version February 19, 2018
Preprint typeset using LaTeX style AASTeX6 v. 1.0

NON-ZEEMAN CIRCULAR POLARIZATION OF MOLECULAR SPECTRAL LINES IN THE ISM

M. A. Chamma[1], M. Houde[1], J. M. Girart[2] and R. Rao[3]
[1]Department of Physics and Astronomy, The University of Western Ontario, London, ON, N6A 3K7, Canada
[2]Institut de Ciències de l'Espai (IEEC-CSIC), Can Magrans, S/N, E-08193 Cerdanyola del Vallès, Catalonia, Spain
and
[3]Submillimeter Array, Academia Sinica Institute of Astronomy and Astrophysics, 645 N. Aohoku Place, Hilo, HI 96720, USA

Abstract

Understanding the role of magnetic fields in star-forming regions allows us to test ideas about free-fall collapse and support mechanisms in molecular clouds, filling in details about the star formation process. Magnetic fields are commonly probed through linear polarization observations from dust continuum and/or molecular spectral transitions, and analysed through the Davis-Chandrasekhar-Fermi method. For molecular lines circular polarization is usually ignored, largely because of difficulty in measurement and its assumed irrelevance. We find in archival data of the Submillimeter Array (SMA[a]) several examples of circular polarization in common molecular tracers, most notably CO. This circular polarization possibly arises from anisotropic resonant scattering implying that some background linearly polarized flux is being converted to circular polarization. We find circular polarization in NGC7538, IRC+10216 and Orion KL to sufficient degrees that we believe the presence of circular polarization in these spectral lines is widespread for such objects, implying that an important piece of information has been missed when studying magnetic fields through linear polarization from molecular spectral lines in the interstellar medium.

1. INTRODUCTION

This section will cover the background of measuring magnetic fields in the interstellar medium (ISM) and Section 2 will discuss the issues that arise when doing polarimetry with radio interferometry, focusing specifically on circular polarization (CP). Section 4 presents archival observations of four objects made with the Submillimeter Array (SMA) on Mauna Kea and makes the case that these circular polarization detections are real and physical. Section 3 will give in detail our scheme for correcting a spurious source of CP that arises with the SMA. Finally in Section 5 we will highlight the significance of these CP detections and summarize relevant research.

Since we can only measure the radiation from star-forming regions astronomers use polarimetry to infer properties like the direction and magnitude of the magnetic field. The Davis-Chandrasekhar-Fermi (DCF) (Chandrasekhar & Fermi 1953) is one method that uses the dispersion of polarization angles (PA) of linear polarization (LP) to find the magnitude and direction of the plane-of-the-sky component of the magnetic field. The presence of a magnetic field leads to linearly polarized radiation because dust molecules will align themselves to the field. The aligned particles emit radiation that is linearly polarized. Aligned dust will also absorb radiation whose polarization is aligned with its long axis, acting as a sort of polarizing grid. Thus measuring the amount of linear polarization in the infrared continuum tells us about the degree to which the dust is aligned with the magnetic field which in turn tells us about the strength of the magnetic field (Chandrasekhar & Fermi 1953; Crutcher 2012).

The alignment of molecules and their interaction with the ambient magnetic field can cause that molecule's transitions to be linearly polarized by a few percent through the Goldreich-Kylafis effect (Goldreich & Kylafis 1981). As with dust, the PA associated with the linear polarization in the spectral line can be measured and used to infer properties of the magnetic field through a dispersion analysis (Chandrasekhar & Fermi 1953; Crutcher 2012).

A significant amount of unexpected circular polariza-

[a] The Submillimeter Array is a joint project between the Smithsonian Astrophysical Observatory and the Academia Sinica Institute of Astronomy and Astrophysics and is funded by the Smithsonian Institution and the Academia Sinica.

tion was reported by Houde et al. (2013) in a rotational transition of CO using the Caltech Submillimeter Observatory (CSO), a common tracer of the magnetic field (Crutcher 2012). The presence of circular polarization in a molecular transition can be explained with Zeeman splitting for some molecules/transitions possessing a significant magnetic momeny (e.g., CN), but CO is highly insensitive to the Zeeman effect. In addition, the observed Stokes V profile in Orion KL was positive and symmetric, which is also unexpected since Zeeman splitting usually gives rise to an antisymmetric Stokes V profile. To explain this detection a model was proposed whereby linearly polarized light is converted to circularly polarized light through anisotropic resonant scattering (ARS) (Houde et al. 2013; Houde 2014). This was further tested in IC443 by Hezareh et al. (2013) where the measured circularly polarized flux of CO lines ($J = 2 \rightarrow 1$) and ($J = 1 \rightarrow 0$) were 're-added' into the measured linearly polarized flux to correct the polarization angles. They found that the polarization angles obtained from the CO tracers only agreed with those obtained from dust polarimetry after the circularly polarized flux was accounted for. If ARS is common to other objects then using linear polarization in CO as a tracer of the magnetic field will have a systematic error unless the circular polarization of CO's lines are also measured. The goal of this paper is to show several examples of such circular polarization.

2. MEASUREMENT OF CP WITH RADIO INTERFEROMETRY

The measurement of circular polarization is challenging to calibrate, especially when using radio interferometers like the SMA or ALMA. The SMA polarimeter uses a quarter-waveplate (QWP) to convert incident linearly polarized light to circularly polarized light primarily to measure linear polarization. While not its intended use, the QWP can work the other way to measure CP: incident CP is converted to LP and then measured by the receivers. ALMA on the other hand uses linear feeds and measures the linearly polarized light directly. While both types of feeds can be used to measure circular polarization, the calibration process is different Sault et al. (1996). Currently ALMA does not support measuring Stokes V reliably. The SMA has been used to take precise measurements of CP in Sgr A* as reported in Muñoz et al. (2012). For a discussion on measuring CP with radio interferometry and on design choices at the SMA (such as the choice of converting from linear- to circular-polarization and vice-versa) see Hamaker et al. (1996); Marrone et al. (2008).

2.1. *Linear vs. Circular Feeds*

To illustrate briefly the differences between the two feed types consider the following: with orthogonal circular polarization bases, the Stokes V parameter for a beam of light is defined by $V = \langle E_L^2 \rangle - \langle E_R^2 \rangle$, where E is the electric field vector and L and R correspond to the orthogonal left-CP and right-CP bases. With orthogonal linear bases Stokes V is defined by $V = -2\mathrm{Im}(E_x E_y^*)$ where x and y are the linear bases. In the circular case we take the difference of two measured intensities while the linear feed case requires us to measure the phase of the electromagnetic wave.

Now when the measurement is made with interferometry it is the visibilities –the correlated waveforms between a pair of antennae– that are measured. In the circular case the Stokes V visibility is roughly $\mathcal{V}_\mathrm{V} \propto \mathcal{V}_{RR} - \mathcal{V}_{LL}$ where $\mathcal{V}_{RR}$ and $\mathcal{V}_{LL}$ are the visibilities obtained from correlating two antenna measuring right-CP and left-CP respectively. In the linear feed case the Stokes V visibility is coupled with the Stokes Q and U visibilities (see Section 4.1 of Thompson et al. 2001). This means the Stokes Q and U of any calibration object must be measured as well. This is not possible with the SMA setup.

3. SQUINT CORRECTION

Here we describe spurious Stokes V that arises when using the SMA and our scheme for correcting it. This instrumental Stokes V comes from a slight pointing offset between the left- and right-handed CP beams.

The archival data used was in all cases observed with the goal of measuring linear polarization (i.e., the Stokes Q and Stokes U parameters). On the SMA this is done with a quarter-waveplate placed in front of the linear receivers to convert incident circular polarization (CP) to linear polarization. While this method suffers from the errors that arise when subtracting two large measurements from each other, it avoids having to solve for the linear polarization terms of calibration objects when obtaining Stokes V (Marrone et al. 2008; Thompson et al. 2001). Obtaining Stokes V from the visibilities measured with circular feeds is done as follows. Given antennae a and b, the Stokes V visibility in the circular feed case is found through (Muñoz et al. 2012):

$$\mathcal{V}_V \simeq \frac{1}{2}\Big\{\mathcal{V}_{RR}/(g_{Ra}g_{Rb}^*) - \mathcal{V}_{LL}/(g_{La}g_{Lb}^*)\Big\}, \qquad (1)$$

where the right-handed CP and left-handed CP visibilities are $\mathcal{V}_{RR}$ and $\mathcal{V}_{LL}$ and are measured by orienting the quarter-waveplate that is placed in the beam of the antennae and correlating the responses of the antennae (Marrone et al. 2008). The complex gain factors for each polarization for each antennae are g_{Ra}, g_{Rb}, g_{La} and g_{Lb} with 'R' and 'L' for right- and left-CP, respectively. Because the Stokes V visibility is found by taking the dif-

ference of two beams a slight offset gives rise to pairs of positive and negative peaks of Stokes V, as shown in Figure 1. This offset likely arises because of slight differences in the index of refraction of the quarter-waveplate when it is rotated, but has not been studied with the SMA as far as we know.

Because the visibilities are the Fourier transform of the intensity map, an offset in image space is equivalent to a complex factor in visibility space that can be absorbed into the gain coefficients.

Consider a map $I(l,m)$ that represents the true intensity I at angular position l and m. An interferometer samples the Fourier transform of this map $V(u,v) = \int\int e^{-iul}e^{-ivm}I(l,m)dldm$. If the instrument introduces an offset from some unknown position (l_0, m_0) then the final image we calculate is shifted such that $I'(l,m) = I(l-l_0, m-m_0)$ and the Fourier transform of the shifted map is $V'(u,v) = \int\int e^{-iul}e^{-ivm}I(l-l_0, m-m_0)dldm$. Changing variables with $\alpha = l - l_0$ and $\delta = m - m_0$ we see

$$V'(u,v) = \int\int e^{-iu(\alpha+l_0)}e^{-iv(\delta+m_0)}I(\alpha,\delta)d\alpha d\delta$$

$$V'(u,v) = e^{-iul_0}e^{-ivm_0}\int\int e^{-iu\alpha}e^{-iv\delta}I(\alpha,\delta)d\alpha d\delta$$

$$V'(u,v) = e^{-iul_0}e^{-ivm_0}V(u,v) \equiv g_{\rm offset}V(u,v) \quad (2)$$

This means that an offset will introduce a complex factor ($g_{\rm offset}$) to the true visibilities. It is therefore easiest to correct for the offset in visibility-space by using *Miriad* (Sault et al. 1995) to solve for the gain coefficients on each beam. Specifically the process is:

1. Observations are calibrated for gain and phase in the usual way using calibration observations of 'good' sources (usually quasars like 3C84, 3C454, etc.) (See Miriad User Guide Sault et al. (2008))

2. Visibilities are split into line-free continuum data and line data. These are then mapped and used to obtain CLEAN models

3. The separate continuum and line data are further split into LL and RR visibilities. *Miriad*'s `selfcal` is used on the continuum data to solve for the gain coefficients of each antenna and each polarization (L or R). This is done by minimizing the difference between measured visibilities $\mathcal{V}_{ij}$ of antennae i and j and model visibilities $\hat{\mathcal{V}}_{ij}$ according to $\epsilon^2 = \sum|\mathcal{V}_{ij} - g_i g_j^* \hat{\mathcal{V}}_{ij}|^2$ for each of the correlations LL and RR (Sault et al. 2008; Schwab 1980). The model visibilities used are those found earlier.

4. The gains found from the continuum LL data is then applied to the line LL data, similarly for the RR continuum and line data.

5. The different visibilities (LL, RR, RL, LR) are recombined and inverted to produce corrected maps. Spectra can be obtained either from the corrected visibilities or the maps.

Figure 1 shows maps before and after this correction is applied.

4. OBSERVATIONS

We collected radio interferometric polarimetry observations from the Submillimeter Array (SMA) archive that had been measured using the circular feeds, a similar setup to that used by Muñoz et al. (2012) to measure circular polarization in Sgr A*. Because the archival observations were not taken with measurements of circular polarization in mind the SNR is often low, and we had to average velocity channels to increase the SNR at the cost of spectral resolution. This generally increases the SNR from 3-4 to 6-10.

The four objects we present here are Orion KL, NGC7538, IRAS2a in NGC1333 and IRC+10216. The first three are well-known star-formation regions while IRC+10216 is an evolved carbon star. We find significant Stokes V signals in all objects except for NGC1333.

The visibility data are corrected for beam squint, an instrumental artifact that gives rise to spurious Stokes V signals. Squint typically causes distinct pairs of positive and negative peaks of Stokes V throughout the inverted image. Maps are then made of the continuum and lines for each object. The squint correction is confirmed visually by inspecting the Stokes V maps, where we see the pairs of peaks largely disappear. More details on the squint correction will be given in Section 3.

Figure 2 shows corrected Stokes I and Stokes V spectra (left) obtained at the peak of Stokes V on the corresponding maps (right). A comparison of Stokes V spectra before and after correction are shown in Figure 3. Notice in all cases the Stokes V signal decreases after squint correction. Stokes V can also be found in the average of all the visibility data, though the significance is 3-5σ in that case compared to approximately 6-10σ when the spectra is taken from the inverted maps. This indicates the detections are not simply the result of the inversion process that creates the maps. We present here only the map spectra. In general the peaks of Stokes I and Stokes V are not at the same map position.

In Orion KL the lines of CO ($J = 3 \rightarrow 2$ at 345.8GHz) and SiO ($J = 8 \rightarrow 7$ at 347.3GHz) are both bright (peak Stokes I of around 20 Jy/beam and 55 Jy/beam respectively; not shown) and both show Stokes V signals. The CO Stokes V signal has an antisymmetric structure

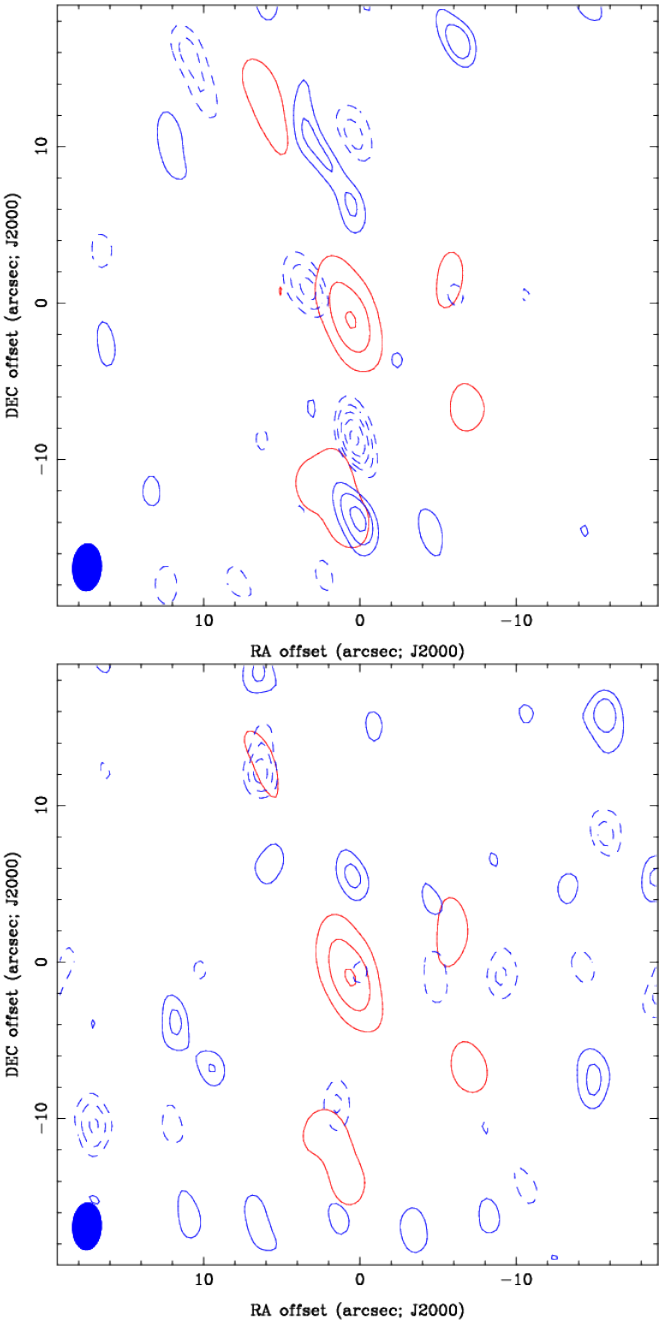

Figure 1. **try getting the corrected solution with different bandpasses** Map of the continuum around 345GHz in Orion KL before (top) and after (bottom) squint correction. Red contours are Stokes I, blue contours are Stokes V. Dashed lines denote negative values, solid lines denote positive values. Note the multiple pairs of positive and negative Stokes V peaks. These largely disappear after correction. The contour scales on both maps are identical. Red Stokes I contours are at 15%, 35%, 55%, 75% and 95% of the peak intensity. Blue Stokes V contours are at -8, -7, -6, -5, -4, -3, -2, 2, 3, 4, 5, 6, 7 and 8σ levels.

while the SiO Stokes V signal is purely negative. Figure 5 shows the peak Stokes V signal of the SiO line. We checked the average of all the visibilities (average over all antennae baselines and all time intervals) and found that the CO Stokes V signal is more intense than the SiO Stokes V signal, and the Stokes I intensities after averaging the visibilities were approximately 50 Jy and 75 Jy for CO and SiO respectively. If the Stokes V signal were purely leakage from Stokes I then we would expect to see an SiO Stokes V signal that is stronger than the CO Stokes V signal, but we do not.

In IRC+10216 we again see Stokes V in the CO ($J = 3 \rightarrow 2$) but also several signals in CS ($J = 7 \rightarrow 6$), SiS ($J = 19 \rightarrow 18$), and $H^{13}CN$ ($J = 4 \rightarrow 3$). These lines and their frequencies are listed in Table 2.

In NGC7538 there was a strong Stokes V detection in CH_2CO at 346.6 GHz that completely disappeared after correction. The Stokes V signal in CO ($J = 3 \rightarrow 2$) at 345.8 GHz decreased in intensity but is still extremely prominent.

Finally Figure 4 shows no detection in NGC1333, with only a weak detection of CO in Stokes I.

When assessing the Stokes V detections we consult the map for obvious pairs of positive/negative peaks that would indicate beam offset and therefore a false Stokes V signal. The maps are integrated over a narrow frequency band of approximately 2 MHz so any peaks that exist should not be washed out by noise in adjacent channels. In the maps for Orion KL and IRC+10216 shown in Figure 2 there are no negative peaks around the peak of Stokes V. However in NGC7538 there is quite a large negative Stokes V peak near our chosen peak that may indicate squint. The top panel of Figure 1 shows what 'squint peaks' look like (we know these peaks are from squint because they disappear after correction) and the pairs tend to resemble each other in shape. The pair of peaks around our chosen peak in NGC7538 however have distinct shapes. The worst case here is that the signal is entirely squint but on the other hand the signal may be a mixture of real and heavily affected by squint. The detections in Orion KL and IRC+10216 are more reliable.

Table 1 shows a summary of the objects presented and related information.

5. DISCUSSION

Are these detections of CP in the archival SMA data shown real or are they instrumental artifacts? This is our chief concern because of the difficulty of calibrating CP measurements and because the measurements presented here were not made with any special considerations for calibrating CP as in the observation of Sgr A* reported in Muñoz et al. (2012). We repeat here the arguments made in Section 4 that these detections are

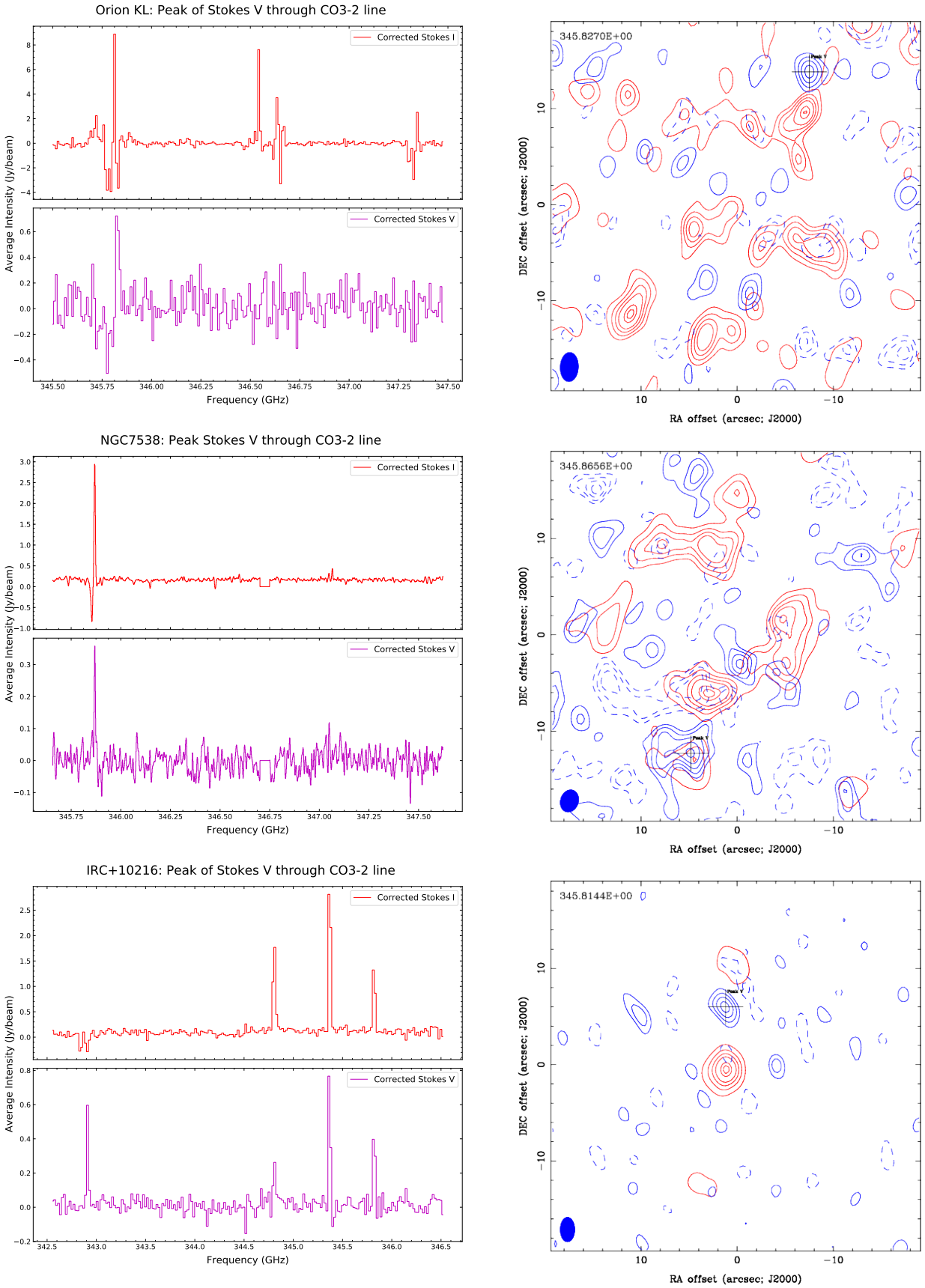

Figure 2. Corrected maps of the CO $J = 3 \rightarrow 2$ line (345.8GHz) and corrected spectra for Orion KL, NGC7538, IRC+10216. ***Spectra*:** *Miriad*'s `maxfit` is used on the CO map to obtain the location on the image where the Stokes V signal at 345.8GHz is maximum, and a spectra is obtained through that point. The cross on the map denotes the location of that peak. The red line is Stokes I and the blue is Stokes V. The spectrum for NGC7538 is Hanning smoothed by a length of 15. ***Maps*:** Blue contours are Stokes V and are shown at the -4, -3, -2, 2, 3, 4σ levels. The RMS error for each Stokes V map is found using *Miriad*'s `imstat` command: σ =0.30, 0.15, and 0.17 Jy/beam, respectively. Dark red contours are Stokes I and the levels are 15%, 30%, 45%, 60%, 85% and 95% of the maximum. The value in the top left is the central frequency of the mapped signal and the map is integrated over a narrow bandwidth of ∼2 MHz.

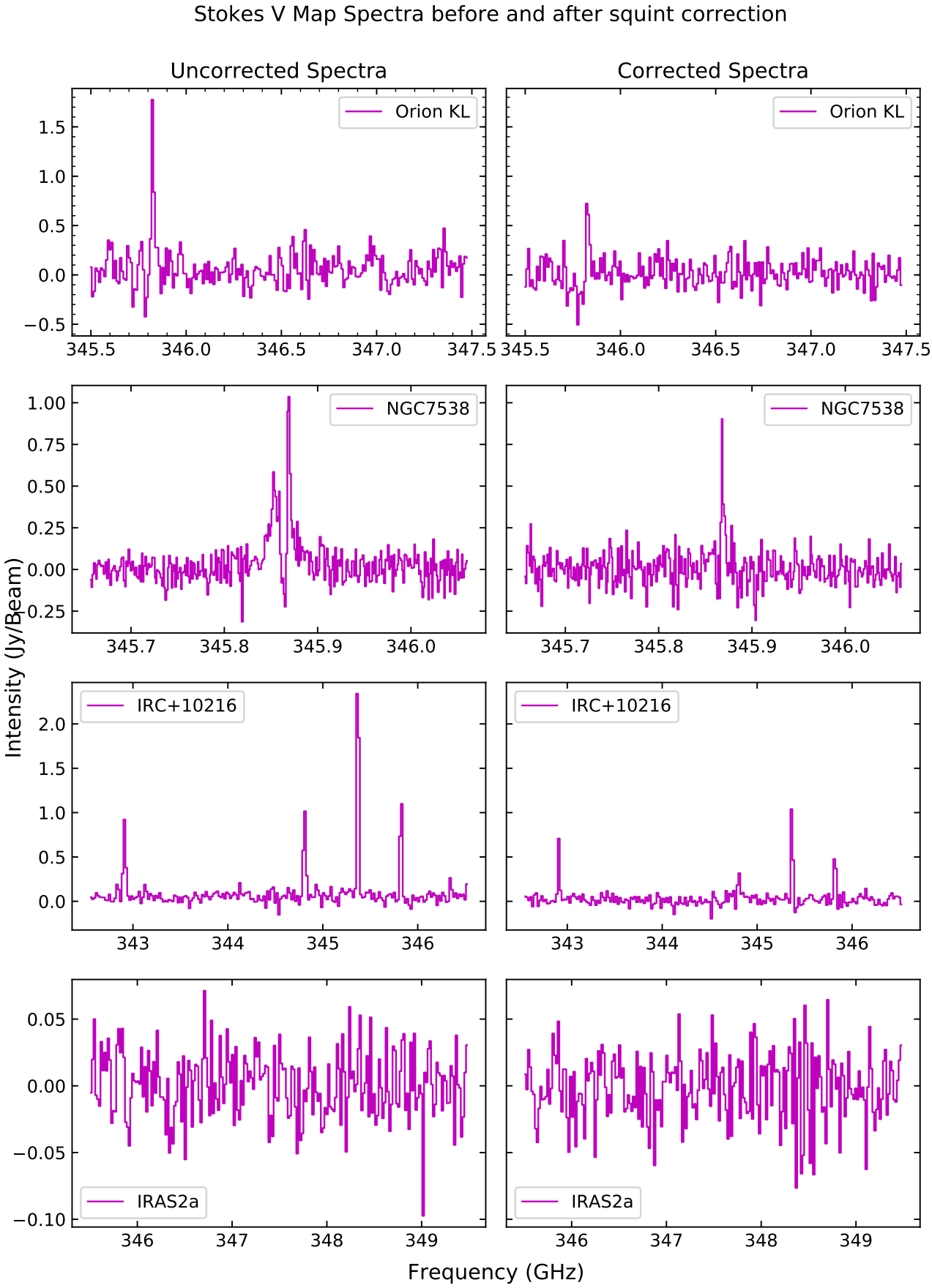

Figure 3. Stokes V spectra of all objects before and after squint correction. *Miriad*'s `maxfit` is used on the CO map for each respective object to obtain the location in the image where the Stokes V signal at 345.8GHz is maximum, and a spectra is obtained through that point. Note that the Stokes V signal decreases in all cases after squint correction.

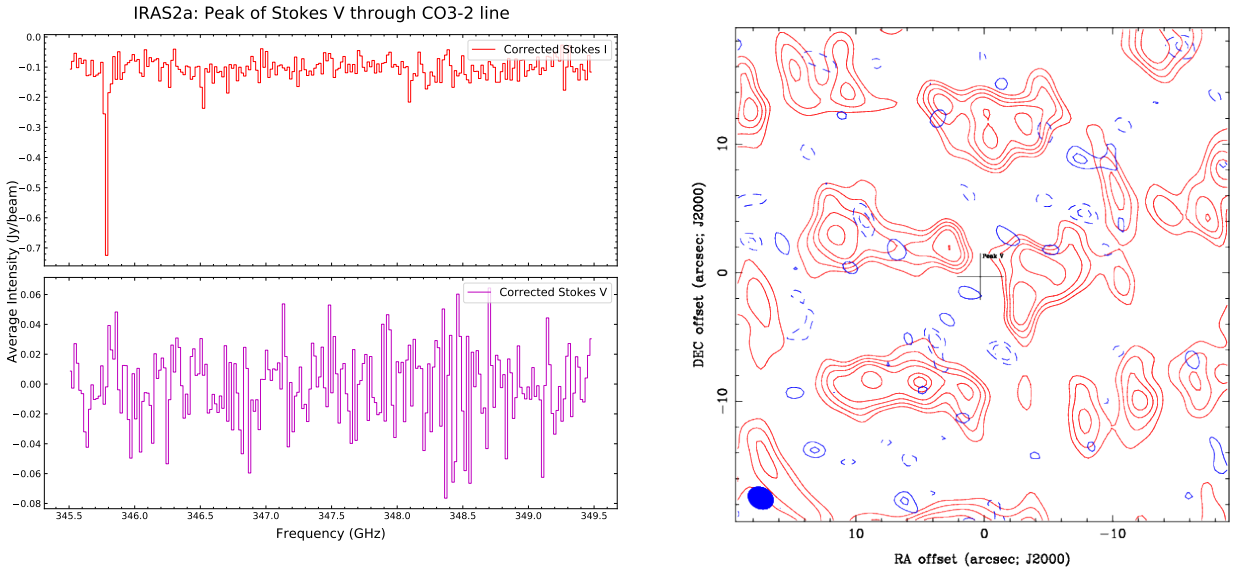

Figure 4. Corrected maps of the CO $J = 3 \rightarrow 2$ line and corrected spectrum for NGC1333 (IRAS2a). No significant Stokes V signal is detected here, probably because the object is too dim. Contours are the same levels as in Figure 2 and the spectrum is obtained the same way.

Object	Coordinates (J2000)	Array Configuration	Date Observed
Orion KL	RA $05^h35^m14.501^s$ Dec -05°22'30.40"	Compact	2008-01-06
NGC7538	RA $23^h13^m44.771^s$ Dec +61°26'48.85"	Compact	2014-10-28
IRC+10216	RA: $09^h47^m57.381^s$ Dec +13°16'43.70"	Compact	2009-11-24
NGC1333	RA $03^h28^m55.580^s$ Dec +31°14'37.10"	Compact	2010-10-14

Table 1. Summary of Archival Observations Used

real. We then discuss earlier detections of CP and summarize how ARS can explain the detections presented in this work.

Firstly we take the average of all the visibility data and note that the peak Stokes V is not proportional to the peak Stokes I at any particular frequency –a large Stokes I at 347.25GHz for example does not indicate a corresponding peak in Stokes V. This property indicates that there isn't significant leakage of Stokes I into Stokes V. This is true in Orion KL (where CO ($J = 3 \rightarrow 2$) and SiO ($J = 8 \rightarrow 7$) are the strongest lines). This also seems to be true in the visibilities of IRC+10216: the CS ($J = 7 \rightarrow 6$) and SiS ($J = 19 \rightarrow 18$) lines have similar strengths but the Stokes V at SiS ($J = 19 \rightarrow 18$) is twice as intense. However in the same object $H^{13}CN$ ($J = 4 \rightarrow 3$) and CO ($J = 3 \rightarrow 2$) have Stokes V intensities that appear proportional to their Stokes I intensity (stronger I means stronger V).

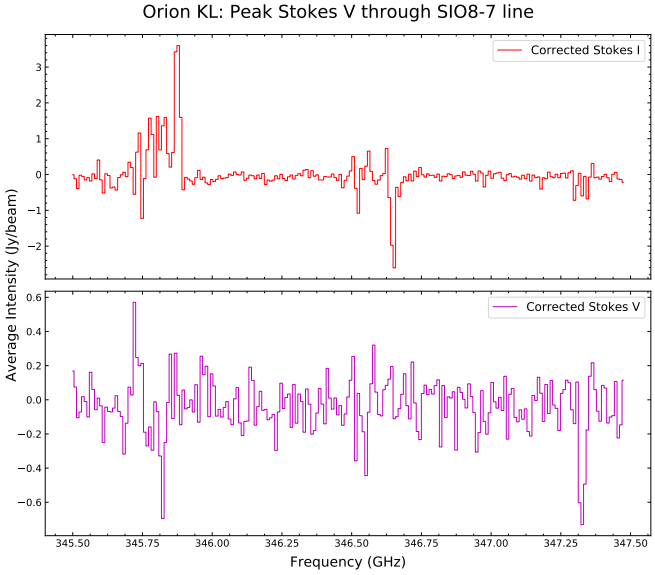

Figure 5. Peak Stokes V signal for the SiO ($J = 7 \rightarrow 8$ at 347.3 GHz) transition in Orion KL. Note there is also a strong Stokes V signal in the CO ($J = 3 \rightarrow 2$ at 345.8 GHz) transition here. The SiO signal is purely negative but the CO signal is antisymmetric.

We also note that the shapes of the Stokes V signals vary across the frequency band and interpret this to mean that the signals are not instrumental in nature. For example Figure 5 shows a spectrum from Orion KL with Stokes V in CO and SiO. The SiO signal is purely negative (indicating only left-circular polarization) but the CO signal is antisymmetric and is initially positive and then becomes negative, indicating the presence of both LCP and RCP. This has a physical explanation

Object	Line	(GHz)	Stokes V (Jy/beam)
Orion KL	CO $J = 3 \rightarrow 2$	345.8	0.65
	SiO $J = 8 \rightarrow 7$	347.3	-0.65
NGC7538	CO $J = 3 \rightarrow 2$	345.8	0.85
IRC+10216	CS $J = 7 \rightarrow 6$	342.88	0.6
	SiS J =19→18	344.78	0.2
	$H^{13}CN$ J =4→3	345.34	0.8
	CO $J = 3 \rightarrow 2$	345.8	0.4
NGC1333 (IRAS2a)	CO $J = 3 \rightarrow 2$	345.8	None

Table 2. Summary of corrected Stokes V signals found. The beam size is determined by the configuration of the antennae array. An intensity for the peak of the Stokes V signal is only given if the peak is noticeably higher than the noise level. The intensity quoted for CO in NGC7538 is before smoothing is applied.

using the ARS model in terms of blue-shifted and red-shifted scattering populations that will be considered in Section 5.2. We know of no instrumental mechanism for producing such a signature. This argument only applies to Orion KL. In the other objects the Stokes V signal is always positive.

In the case of IRC+10216, an evolved carbon star with an extended envelope, we note that the peak of Stokes V in the CO ($J = 3 \rightarrow 2$) map (bottom-right panel of Figure 2) is roughly 6" away from the Stokes I emission, and were concerned that the Stokes V peak was not even on the object. From single-dish CO ($J = 2 \rightarrow 1$) observations of the shell around IRC+10216 we find the radius of the CO shell to be 50" (Fig. 1 of Cernicharo et al. 2015), indicating that the Stokes V signal is indeed on the object.

Spatial filtering due to the resolution of the interferometer explains the much smaller radius of IRC+10216 in the observations presented here and also explains the frequent occurences of negative Stokes I in almost all the spectra shown in Figures 2, 4, and 5. The largest resolvable object by an interferomter is determined by the length of the shortest baseline, meaning that large scale emission can be invisible to the interferometer. For example in Orion KL the CO ($J = 3 \rightarrow 2$) Stokes I emission is large and extended. If then the Stokes V signal comes from smaller more localized areas, we would observe peaks of Stokes V as shown and only a portion of the Stokes I that is present. The rest of the Stokes I signal would be filtered away which could shift the zero-level to smaller values. Fluctuations in Stokes I would then appear to have negative values. ***details, maybe an equation***

Finally we checked and confirmed that there were no Stokes V signals in the continuum larger than those found at molecular lines like CO and SiO. Finding a large signal in the continuum could indicate the data is suffering from instrumental artifacts since we only expect conversion of linear to circular polarization at the frequencies of molecular transitions. This is not the case: we only find Stokes V peaks at frequencies that correspond with emission from molecular lines and there is no significant CP in the continuum.

For these reasons we believe the CP reported here while quite probably contaminated with instrumental effects are real and originate from each of these objects. It is thus important to develop the instrumentation and improve the measurement and calibration of CP for future studies of magnetic fields using polarimetry.

5.1. *Earlier Detections*

Circular polarization in a spectral line of a Zeeman insensitive molecule was first reported in Houde et al. (2013) where roughly 2% CP was detected in the ^{12}CO ($J = 2 \rightarrow 1$) line at 230.5 GHz in Orion KL using the CSO. The CP signal was positive and symmetric ("∩"-shaped). The observation was repeated three months after the first measurement to confirm the result wasn't spurious, with similar results. Additionally the strong line of HCN ($J = 3 \rightarrow 2$) at 265.9 GHz in Orion KL was measured and no CP higher than the 0.1% level was detected. The detection in CO and the absence of a detection in HCN indicates that the CSO observations were not suffering from leakage into Stokes V and highlights the CO molecule as a source of non-Zeeman CP. In all the objects presented here we find CP in ^{12}CO ($J = 3 \rightarrow 2$) at 345.8 GHz (except for in NGC1333 where the CO line is weak). This is consistent with the original 2013 detection.

In follow up work Hezareh et al. (2013) examined the supernova remnant IC 443 using dust polarimetry with PolKa at APEX and polarization maps of ^{12}CO ($J = 2 \rightarrow 1$) and ($J = 1 \rightarrow 0$) taken with the IRAM 30m telescope. They found that initially the linear polarization maps of dust and CO differed greatly in their polarization angles. Expecting that there was conversion of linear to circular polarization due to ARS, the CO Stokes V flux was then reinserted into the CO Stokes U flux. The resulting CO map's polarization angles now agreed very well with the polarization angles in the dust map (Fig. 9 of Hezareh et al. 2013). This result gives strong support for a conversion from linear to circular polarization.

5.2. *Anisotropic Resonant Scattering*

Anisotropic resonant scattering was the mechanism first proposed by Houde et al. (2013) to explain the presence of CP in the transitions of CO, but failed to explain the observed positive and symmetric "∩"-shaped Stokes V profile. In a follow up paper Houde (2014) considered observations of Stokes V in SiO masers and showed that different profile shapes easily arose if there were populations of scattering foreground molecules slightly outside of the velocity range of the line. For example in that case a blue-shifted scattering population of molecules results in a negative "∪"-shaped profile and a red-shifted population results in a positive "∩"-shaped profile. The presence of both a blue- and red-shifted population results in an antisymmetric "S"-shaped profile like the one seen in the top left panel of Figure 2.

The basic principle of ARS can be illustrated by considering linearly polarized radiation oriented at some angle θ to the foreground magnetic field. The incident and scattered radiation can be written in terms of the n-photon states as (Houde et al. 2013)

$$\begin{aligned} |\psi\rangle &= \quad \alpha|n_{||}\rangle + \beta|n_{\perp}\rangle \\ |\psi'\rangle &\simeq \alpha e^{i\phi}|n_{||}\rangle + \beta|n_{\perp}\rangle \end{aligned}$$

where $\alpha = \cos(\theta)$, $\beta = \sin(\theta)$ and ϕ is a phase shift incurred after multiple scattering events. Following the definitions of the Stokes parameters and using the appropriate bases the Stokes parameters for the scattered radiation can be found to be

$$\begin{aligned} I &= \quad \alpha^2 + \beta^2 \\ Q &= \quad \alpha^2 - \beta^2 \\ U &= 2\alpha\beta\cos(\phi) \\ V &= 2\alpha\beta\sin(\phi) \end{aligned}$$

This implies that Stokes U is lost to Stokes V. A calculation of the phase shift ϕ incurred due to anisotropic resonant scattering can be found in Houde et al. (2013).

6. CONCLUSION

We took polarimetric observations from the SMA archive of Orion KL, IRC+10216, NGC7538 and NGC1333 and examined them for signals of circular polarization. The data were corrected for squint, a source of false Stokes V signals that arises due to a slight misalignment in the beams used to obtain Stokes V when using the SMA's quarter-waveplate-based polarimeter. We found evidence of significant Stokes V in Orion KL, IRC+10216 and NGC7538 in the transitions of CO ($J = 3 \rightarrow 2$), SiO ($J = 8 \rightarrow 7$), CS ($J = 7 \rightarrow 6$), SiS ($J = 19 \rightarrow 18$) and $H^{13}CN$ ($J = 4 \rightarrow 3$), but because of low SNR in the spectra we could not model the shape of Stokes V. We also obtained much higher percentages of polarization than expected (ranging from 6-30% for V/I) due to the spatial filtering of large scale emission.

Theories that explain the presence of non-Zeeman circular polarization in molecular spectral lines rely on the conversion of background linear polarization. The several detections in multiple lines and objects presented here indicate that such an effect is likely widespread and common.

Taking precise observations of CP along with LP and correcting for this conversion effect is therefore a critical step in polarization studies of the magnetic field in the interstellar medium.

REFERENCES

Cernicharo, J., Marcelino, N., Agúndez M., & Guéllin, M. 2015 A&A, 575, A91

Chandrasekhar, S., & Fermi, E. 1953 ApJ, 118, 113

Crutcher, R. M. 2012 Annu. Rev. Astron. Astrophys, 50, 29-63

Goldreich, P., Kylafis, N. D. 1981 ApJ, 243, L75-L78

Hamaker, J. P., Bregman, J. D., & Sault, R. J. 1996 A&A Suppl. Ser., 117, 137-147

Hezareh, T. J., Wiesemeyer, H., Houde, M., Gusdorf, A., Siringo, G. 2013 A&A, 558, A45

Houde, M., Hezareh, T., Jones, S., & Rajabi, F. 2013 ApJ, 764, 24

Houde, M. 2014 ApJ, 795, 27

Muñoz, D. J., Marrone, D. P., Moran, J. M., & Rao, R. 2012 ApJ, 745, 115

Marrone D. P. & Rao R. 2008, Proc. SPIE 7020, 70202B

Sault, R. J., Teuben, P. J. & Wright M. C. H. 1995 ADASS IV, ASP Conference Series, 77, 433-436

Sault, R. J., Hamaker, J. P., & Bregman, J., D. 1996 A&A Suppl. Ser., 117, 149-159

Sault, R. J., Killeen, N. 2008, Miriad Users Guide, Australia Telescope National Facility

Schwab, F. R. 1980, Proc. SPIE 0231, Intl Optical Computing Conf I

Thompson, A. R., Moran, J. M., & Swenson Jr, G. W. 2001, Interferometry and synthesis in radio astronomy (John Wiley & Sons)

Vallée, J. P. 2011, New Astronomy Reviews 55, 23–90